Computational prediction of phytochemical inhibitors against the cap-binding domain of Rift Valley fever virus

Ishwarya Muralitharan
The Institute of Mathematical Sciences (IMSc)
Ajaya Kumar Sahoo
The Institute of Mathematical Sciences (IMSc)
Priya Dharshini Augusthian
The Institute of Mathematical Sciences (IMSc)
Areejit Samal (asamal@imsc.res.in)
The Institute of Mathematical Sciences (IMSc)

Research Article

Keywords: Rift Valley fever virus, Phytochemical inhibitors, Cap-binding domain, Molecular dynamics, Molecular docking, Virtual screening

Posted Date: May 10th, 2023

DOI: https://doi.org/10.21203/rs.3.rs-2902753/v1

Additional Declarations: No competing interests reported.

Version of Record: A version of this preprint was published at Molecular Diversity on July 23rd, 2023. See the published version at https://doi.org/10.1007/s11030-023-10702-x.

Abstract

Rift Valley fever is a zoonotic disease that can spread through livestock and mosquitoes, and its symptoms include retinitis, photophobia, hemorrhagic fever and neurological effects. The World Health Organization has identified Rift Valley fever as one of the viral infections that has potential to cause a future epidemic. Hence, efforts are urgently needed toward development of therapeutics and vaccine against this infectious disease. Notably, the causative virus namely, the Rift Valley fever virus (RVFV), utilizes the cap-snatching mechanism for viral transcription, rendering its cap-binding domain (CBD) as an effective antiviral target. To date, there are no published studies towards identification of potential small molecule inhibitors for the CBD of RVFV. Here, we employ a virtual screening workflow comprising of molecular docking and molecular dynamics (MD) simulation, to identify 5 potential phytochemical inhibitors of the CBD of RVFV. These 5 phytochemical inhibitors can be sourced from Indian medicinal plants, *Ferula assa-foetida, Glycyrrhiza glabra* and *Leucas cephalotes*, used in traditional medicine. In sum, the 5 phytochemical inhibitors of the CBD of RVFV identified by this purely computational study are promising drug lead molecules which can be considered for detailed experimental validation against RVFV infection.

Introduction

The zoonotic disease Rift Valley fever is mosquito-borne and is prevalent among humans and animals in sub-Saharan African countries [1, 2]. The name Rift Valley originates from Kenya's Great Rift Valley, where the causative virus for this disease was first identified [3, 4]. The Rift Valley fever virus (RVFV) belongs to the genus *Phlebovirus* and the family *Phenuiviridae* (previously known as *Bunyaviridae*) [5, 6]. RVFV is transmitted to humans via mosquito or by the contamination with infected animal body fluids or tissues [3]. The Rift Valley fever disease has symptoms such as photophobia, headaches, retinitis, encephalitis, hemorrhagic fever, blindness and neurological effects [2, 5]. Originally endemic to sub-Saharan African regions, RVFV has spread outside to the Arabian peninsula in 2000 [7–9]. The World Health Organization (WHO) has expressed the need to accelerate research and development towards effective therapies and vaccines against RVFV, since the virus has potential to cause world-wide outbreak and public health emergency [10, 11]. During the COVID-19 pandemic, there are also reports of Rift Valley fever outbreak in Uganda [12], and more recently in Mauritania [13]. Although, the overall documented human mortality rate for RVFV infections is less than 1% [14], in the case of severe infection, the human mortality rate can steeply increase to 10–20% [15]. In addition, RVFV is potential bioterrorism agent, as the virus can spread easily through mosquitoes and livestock, and thus, necessitating studies towards development of safe therapies against the RVFV infection [16–19].

RVFV is a single-stranded tri-segmented negative-sense RNA virus [20]. The Large (L) and Medium (M) segments of the RVFV genome have negative polarities, while the Small (S) segment of the RVFV genome has ambisense polarity [20–22]. The M segment of the genome encodes for two glycoproteins (Gn and Gc), and a non-structural protein. The non-structural protein is expressed by itself (NSm1) or in fusion with the glycoprotein Gn (NSm2) [23, 24]. In the negative sense, the S segment of the genome

expresses the nucleoprotein (N protein), and in the positive sense, the S segment expresses the non-structural protein NSs [21, 22]. L segment, the largest segment of RVFV genome, expresses L protein which plays an important role in the viral genome replication and mRNA transcription [25–27]. The L protein has an endonuclease domain at the N-terminal region, an RNA-dependent RNA polymerase in the middle and a cap-binding domain (CBD) at the C-terminal region. Generally, in Bunyaviruses such as RVFV, the L protein initiates the transcription process by a cap-snatching mechanism [26, 28, 29]. In the cap-snatching mechanism, the two domains, endonuclease and cap-binding domains, of the L protein are actively involved. CBD recognizes the m^7GTP cap-analogue present in the 5' region of the host cell mRNA. The endonuclease domain of the L protein cleaves off the 5' host mRNA cap which are used as primers in the transcription of viral mRNA in the host cell [24, 28]. In short, the recognition of the host mRNA cap by the CBD of RVFV L protein is crucial for the initiation of viral transcription. Therefore, the CBD of RVFV L protein can serve as an effective drug target for viral inhibition.

Previously, multiple *in vitro* and computational (virtual) screening studies have been published in the literature with the aim of identifying potential inhibitors to combat RVFV infection or against RVFV proteins such as L protein, glycoprotein N (Gn), glycoprotein C (Gc), and Nucleocapsid (N) proteins [30–34, 27, 35, 19]. In particular, Fatima *et al.*, [35] have performed virtual screening of more than 6000 natural products against multiple proteins of RVFV to identify potential natural product inhibitors. However, to date, there is no published study with the aim of identifying potential inhibitors for the CBD of RVFV L protein. In this contribution, we used established computational approaches to identify potential natural product inhibitors for the CBD of RVFV L protein.

Plants or plant-derived products continue to be valuable sources of therapeutics against viral infections [36, 37]. In this direction, some of the authors have previously built, Indian Medicinal Plants, Phytochemistry And Therapeutics (IMPPAT) database [38], a dedicated online resource on the phytochemicals of the Indian medicinal plants. Subsequent to its publication, IMPPAT has been widely-used in virtual screening studies to identify potential phytochemical inhibitors against viruses including SARS-CoV-2 and SFTSV [39–42]. In this virtual screening study, we leveraged a natural product library of 14011 phytochemicals specific to Indian medicinal plants, compiled from IMPPAT and other literature sources, along with established computational methods such as molecular docking and molecular dynamics (MD) simulations, to identify potential inhibitors of the CBD of RVFV L protein.

Methods

Phytochemical library for virtual screening

In this virtual screening study, we considered a list of 14011 phytochemicals compiled from IMPPAT database [38], a phytochemical atlas specific to Indian medicinal plants, and additional phytochemical information compiled from literature specific to traditional Indian medicine [43–57]. At first, we used Lipinski's rule of five (RO5) [58] to evaluate the potential drug-likeness of the 14011 phytochemicals in our chemical library. Using the RO5 filter, 10510 phytochemicals were identified as drug-like in our

chemical library. For these 10510 drug-like phytochemicals, we retrieved the three-dimensional (3D) chemical structure files in .sdf file format from PubChem [59]. Thereafter, the 3D chemical structures of the phytochemicals were energy-minimized using OpenBabel [60] with the MMFF94 force field, and further, were converted to .pdb file format. Afterwards, we used this filtered library of 10510 drug-like phytochemicals for virtual screening.

Preparation of cap-binding domain structure of RVFV L protein

Gogrefe *et al.* [26] have published the x-ray crystal structure of the cap-binding domain (CBD) of RVFV L protein with a resolution of 1.48 Å, and we obtained this published structure (PDB: 6QHG) from Protein Data Bank (PDB) (https://www.rcsb.org/) for this study. For subsequent docking, we prepared the protein structure of the CBD of RVFV L protein by replacing the selenomethionine residues (MSE) with methionine (MET) residues using the Dock Prep tool in UCSF chimera [61]. Hereafter, the prepared structure of the CBD of RVFV L protein is referred to as 'RVFV-CBD' in the text.

Molecular dynamics simulation

We performed MD simulation of the prepared crystal structure of RVFV-CBD using GROMACS 5.1.5 [62] along with the force field CHARMM36 [63]. For the MD simulation, we prepared the system by placing the protein at the center of a dodecahedron box with periodic boundary conditions, and further, the minimum distance of the protein to any of the box edges was set to 12 Å. Thereafter, we solvated and neutralized the system by adding simple point charge (SPC216) water and six chloride (Cl^-) ions. To minimize the energy of the system, we used the steepest descent algorithm with the tolerance for energy minimization set at 100 kJ mol^{-1} nm^{-1}. Thereafter, we performed NVT simulation for 1 ns with 2 fs time step. The temperature of the system during NVT simulation was set to 300 K. After 1 ns of NVT simulation, we performed 1 ns of NPT simulation with 2 fs time step. The pressure of the system in NPT simulation was set to 1 bar. During both NPT and NVT simulations, the positions of the heavy atoms in the protein were restrained using a force constant of 1000 kJ mol^{-1} nm^{-2}. Note that the bond lengths were constrained using the LINCS algorithm [64]. After removing the position restraint, we performed 1 ns of equilibration simulation with 2 fs time step. Finally, we performed MD simulation for 300 ns in quintuplicate (5 replicates). During this 300 ns MD simulation, we employed v-rescale [65] temperature coupling and Parrinello-Rahman [66] pressure coupling method to keep the temperature of the system at 300 K and pressure of the system at 1 bar.

Clustering of the MD simulation trajectories and extraction of the representative protein structures

Clustering of the MD simulation trajectories and extraction of the representative protein structures

In order to perform the clustering of MD simulation trajectories of the free protein, we combined the trajectories from the quintuplicate simulations by considering only the time interval of 100 ns to 300 ns, and thereafter, extracted 10000 frames from the combined trajectory at equal time intervals. Using C_α atoms of the amino acid residues, we next superimposed the extracted frames on the initial frame of the combined trajectory. Thereafter, we performed the clustering of the 10000 frames by considering only the heavy atoms of the active site residues using Jarvis-Patrick method [67, 62]. This clustering led to the identification of 423 clusters, wherein the top 10 clusters represented nearly 32% of the total frames (3190 frames). We extracted 10 protein structures corresponding to the centers of the top 10 clusters, and these 10 protein structures along with the prepared crystal structure were used for ensemble docking. In sum, we performed ensemble docking of 10510 drug-like phytochemicals with 11 protein structures namely, the prepared crystal structure of RVFV-CBD and 10 protein structures corresponding to the top 10 cluster centers.

Molecular docking using AutoDock Vina

We used AutoDock Vina [68] to perform docking of the ligands in the chemical library (i.e., 10510 drug-like phytochemicals) against 11 protein structures of RVFV-CBD (namely, the prepared crystal structure and 10 structures corresponding to the top 10 cluster centers). The 3D structures of ligands and proteins were converted to .pdbqt format from .pdb format using the scripts namely, prepare_ligand4.py and prepare_receptor4.py in AutoDockTools [69], respectively. To perform the docking, the search space center and grid box dimensions were determined manually by considering the critical residues F1713, R1716, Q1717, Y1728 and M1782 in the cap-binding site of the RVFV L protein (Fig. 1). In particular, the grid center was determined in PyMOL [70] by computing the center of mass of the cap-binding site residues across all 11 protein structures considered for docking. Thereafter, we performed the protein-ligand docking in AutoDock Vina with a grid box dimension of 25 Å × 25 Å × 25 Å and exhaustiveness parameter set to 24.

Computation of protein-ligand interactions

To compute the different non-covalent interactions between the protein and the ligand in complex, we considered the best docked pose (lowest binding energy) of the ligand with the protein. Using custom python scripts and pdb-tools [71], we generated the configuration of the protein-ligand complex wherein the ligand is in the best docked pose. As detailed in our previous publications [72, 73], we used custom scripts to analyze and compute different types of non-covalent interactions between the protein and the ligand in the protein-ligand complex. In the computation of the different interactions between the protein and the ligand in the best docked pose, we identified the ligand binding site residues and non-covalent interactions namely, hydrogen bond interactions, hydrophobic interactions and aromatic interactions.

MD simulation of the protein-ligand complexes

To assess the stability of the protein-ligand complexes, we performed MD simulations of 150 ns for the prepared crystal structure of RVFV-CBD in complex with one of the top 9 potential phytochemical inhibitors predicted by docking. For these simulations, we generated the topology parameters for the ligands using SwissParam [74]. We remark that the MD simulation of 150 ns for each protein-ligand complex was carried out using the same parameters as described for the MD simulation of the free protein. Using GROMACS, we computed three different quantities namely, Radius of gyration (R_g), Root Mean Square Deviation (RMSD), and Root Mean Square Fluctuation (RMSF), of the protein or the ligand from the MD simulation trajectories of the protein-ligand complexes.

Binding energy calculation

We computed the binding energies for the 5 potential phytochemical inhibitors predicted to remain stable in the MD simulation of their corresponding protein-ligand complexes using Molecular Mechanics Poisson-Boltzmann Surface Area (MM-PBSA) method. For each of these protein-ligand complexes, we extracted 51 frames from the MD simulation trajectories between 100 ns to 150 ns at a time interval of 1 ns. Thereafter, using g_mmpbsa [75, 76], we computed the binding energy of the ligands in the protein-ligand complexes.

Physicochemical, ADMET and drug-likeness properties of potential phytochemical inhibitors

For the top potential phytochemical inhibitors of RVFV-CBD, we computed the physicochemical properties, drug-likeness properties, and predicted absorption, distribution, metabolism, excretion and toxicity (ADMET) properties using RDKit (https://www.rdkit.org/), SwissADME [77] and ProTox-II [78]. Further, we predicted the chemical classification of the top phytochemical inhibitors using ClassyFire [79] (http://classyfire.wishartlab.com/).

Results and Discussion

Virtual screening workflow to identify potential phytochemical inhibitors of RVFV-CBD

In this study, we followed a virtual screening workflow comprising of five stages to identify potential phytochemical inhibitors of RVFV-CBD. In stage 1, we used Lipinski's RO5 filter to retrieve a subset of 10510 drug-like phytochemicals among 14011 phytochemicals produced by Indian medicinal plants in our chemical library (Methods; Fig. 2). In parallel, the RVFV-CBD protein was subjected to MD simulation in quintuplicate to analyze the conformational diversity of the active site residues. Thereafter, we clustered the MD simulation trajectories of the free protein to retrieve 10 representative protein structures (Methods).

In stage 2, we used AutoDock Vina to perform the docking of the 10510 drug-like phytochemicals against 11 protein structures namely, prepared crystal structure of RVFV-CBD and 10 representative protein structures from clustering of MD simulation trajectories (Methods). From docking computations, we identified the top 10% phytochemicals in terms of their docking based binding energy with respect to each of the 11 protein structures (Fig. 2). In stage 3, we shortlisted 84 phytochemicals (**Supplementary Table S1**) that were common to the top 10% phytochemicals based on docking binding energy for each of the 11 protein structures.

Subsequently, in stage 4 we used relevant criteria such as non-covalent interactions between critical active site residues in protein and ligand in best docked pose, and toxicity of shortlisted phytochemicals to further filter among the 84 phytochemicals (Methods; Fig. 2). Using the non-covalent interaction filter, we shortlisted 37 out of the 84 phytochemicals that form non-covalent interactions with at least three critical active site residues of RVFV-CBD. Thereafter, we used ProTox-II webserver to predict the toxicity of these 37 phytochemicals (**Supplementary Table S2**) that satisfy the non-covalent interaction filter. After imposing the toxicity filter, we obtained 9 phytochemicals (**Supplementary Table S2**) to be non-toxic (Class 5 or Class 6) based on ProTox-II predictions, and these 9 phytochemicals were further considered for stability analysis in stage 5 (Fig. 2).

In stage 5, we assessed the stability of the protein-ligand complexes for each of these 9 phytochemicals using MD simulations. After assessing the results of this MD based stability analysis of protein-ligand complexes of top 9 phytochemical inhibitors, we finally put forward 5 out of the 9 phytochemicals as potential inhibitors for RVFV-CBD (Fig. 2).

Conformational dynamics of RVFV-CBD protein structure

The protein structure of RVFV-CBD consists of seven β-strands, one β-hairpin, and a long α-helix [26]. RVFV-CBD plays an important role in the cap-snatching process during the viral transcription. Five amino acid residues namely, F1713, R1716, Q1717, Y1728 and M1782, which are present in active site of the protein (Fig. 1) were found to interact with the cap-analogue m^7GTP of the host cell mRNA [26]. We performed MD simulation for 300 ns in quintuplicate of the prepared crystal structure of RVFV-CBD to study the conformational dynamics of the free protein. From these quintuplicate simulations, we observed that the RMSD of the C_α atoms of the amino acid residues in the protein structure remains stable with the RMSD values being close to 2 Å throughout the simulation (Fig. 3a). Notably, the RMSD values in the quintuplicate simulations show lesser fluctuations after 100 ns (Fig. 3a). Further, little variation is observed in case of the radius of gyration (R_g) indicating that the protein structure remains compact during the MD simulation (Fig. 3b). Moreover, the RMSF of the amino acid residues in the protein structure also highlights the stability of the free protein during the MD simulation (Fig. 3c). Overall, the analysis of the simulation trajectory of RVFV-CBD shows that the protein structure remains stable and compact during the MD simulation.

Identification of the top phytochemical hits of RVFV-CBD

Using the virtual screening workflow (Fig. 2), we identified top 9 phytochemical hits of RVFV-CBD based on docking binding energy, non-covalent interaction filter and toxicity filter (Table 1). Figure 4 displays the two-dimensional (2D) structures of these top 9 phytochemicals. The 9 phytochemicals belong to four chemical classes namely, 'Coumarins and derivatives', 'Linear 1,3-diarylpropanoids', 'Isoflavonoids' and 'Steroids and steroid derivatives' based on predictions by ClassyFire (Methods; **Supplementary Table S3**).

Table 1
Top 9 phytochemical hits (P1-P9) for RVFV-CBD identified based on molecular docking. For each phytochemical, the table lists the chemical name, PubChem identifier, binding energy of the ligand with the prepared crystal structure obtained from docking in kcal/mol, and the plant source.

Phytochemical symbol	Chemical name	PubChem identifier	Docking binding energy (kcal/mol)	Plant source
P1	Paratocarpin B	CID:42607541	-9.9	*Glycyrrhiza glabra*
P2	Glyinflanin G	CID:15233561	-9.3	*Glycyrrhiza glabra*
P3	Farnesiferol A	CID:7067262	-9.3	*Ferula assa-foetida*
P4	Mogoltadone	CID:14865891	-9.2	*Ferula assa-foetida*
P5	Assafoetidnol A	CID:12041593	-9.2	*Ferula assa-foetida*
P6	Kanzonol B	CID:10881804	-8.9	*Glycyrrhiza glabra*
P7	Gummosin	CID:7092581	-8.6	*Ferula assa-foetida*
P8	Lupinisolone A	CID:14237665	-8.3	*Lupinus albus*
P9	7-Oxostigmasterol	CID:12044013	-8.1	*Leucas cephalotes*

Phytochemicals P1, P2 and P6 have been shown to be present in the plant extract of *Glycyrrhiza glabra* (licorice) (Table 1). In traditional medicine, *Glycyrrhiza glabra*, is used to treat common cold and cough, and the herb used in various systems of medicine such as Ayurveda, Siddha and Unani [80, 81]. Phytochemicals P3, P4, P5 and P7 have been shown to be present in the plant extract of *Ferula assa-foetida* (Table 1). In Ayurveda, *Ferula assa-foetida* is used to treat whooping cough [82]. Phytochemicals P8 and P9 have been shown to be present in the plant extracts of *Lupinus albus* and *Leucas cephalotes*, respectively (Table 1). The herb, *Lupinus albus*, is used in Unani system of medicine [83]. The herb,

Leucas cephalotes, is used in Ayurveda [84], and is reported to have therapeutic effect against common cold and fever [85].

Phytochemical P1, Paratocarpin B is a chalcone that has docking binding energy with prepared crystal structure of RVFV-CBD of -9.9 kcal/mol. Previously, chalcones have been reported to have antiviral properties including against RVFV [86]. In the best docked pose or CBD-P1 complex, Paratocarpin B forms two aromatic interactions with the active site residues F1713 and Y1728. Further, P1 forms hydrophobic interactions with Y1728, P1755, M1782, V1727, F1713, R1716, and Q1717 residues of RVFV-CBD in the best docked pose (Fig. 5; Fig. 6; Table 2).

Table 2

Non-covalent interactions of the top 9 phytochemical hits in the best docked pose with the prepared crystal structure of RVFV-CBD. For each protein-ligand complex, the table lists the amino acid residues in the ligand binding site and amino acid residues which form hydrogen bond interactions, which form hydrophobic interactions, and which form aromatic interactions with the ligand.

Protein-Phytochemical complex	Binding site residues	Hydrogen bond interaction residues	Hydrophobic interaction residues	Aromatic interaction residues
CBD-P1	Q1717, M1782, Y1728, P1755, N1749, Q1753, F1713, R1716, I1747	-	Y1728, P1755, M1782, V1727, F1713, R1716, Q1717	F1713, Y1728
CBD-P2	Q1717, M1782, Y1728, P1755, N1749, Q1753, F1713, R1716, I1747	N1749	Y1728, P1755, M1782, F1713	F1713, Y1728
CBD-P3	M1782, Y1728, P1755, V1727, V1726, F1713, R1716, Q1717	-	Y1728, P1755, V1727, M1782, F1713, R1716	F1713, Y1728
CBD-P4	Y1728, P1755, M1782, V1726, V1727, F1713, R1716, Q1717	-	Y1728, P1755, V1727, M1782, F1713, R1716	F1713, Y1728
CBD-P5	M1782, Y1728, P1755, V1727, V1726, F1713, R1716, Q1717	Y1728	Y1728, P1755, V1727, M1782, F1713, R1716	F1713, Y1728
CBD-P6	Q1717, Y1728, M1782, F1713, R1716, P1755, I1747, N1749	N1749	Y1728, M1782, F1713, R1716, P1755	F1713, Y1728
CBD-P7	M1782, P1755, V1726, V1727, D1781, Y1728, F1713, Q1717, R1716	Y1728	F1713, P1755, M1782, Y1728, R1716, Q1717	F1713, Y1728
CBD-P8	G1752, Y1728, Q1753, V1727, V1726, M1782, F1713, P1755	-	G1752, V1727, Y1728, M1782, F1713	Y1728
CBD-P9	Y1728, P1755, M1782, V1727, Q1753, G1752, F1713, N1749	-	Y1728, P1755, M1782, V1727, G1752, F1713	-

Phytochemical P2, Glyinflanin G, has docking binding energy with prepared crystal structure of RVFV-CBD of -9.3 kcal/mol. In the best docked pose or CBD-P2 complex, P2 forms two aromatic interactions with F1713 and Y1728 residues. Further, there is one hydrogen bond formed between P2 and N1749 residue of RVFV-CBD. Moreover, P2 forms hydrophobic interactions with Y1728, P1755, M1782, and F1713 residues of RVFV-CBD in the best docked pose (Fig. 5; Fig. 6; Table 2).

Phytochemical P3, Farnesiferol A, has docking binding energy with prepared crystal structure of RVFV-CBD of -9.3 kcal/mol. In the best docked pose or CBD-P3 complex, P3 forms hydrophobic interactions with Y1728, P1755, V1727, M1782, F1713, and R1716 residues. Further, P3 forms aromatic interactions with F1713 and Y1728 residues of RVFV-CBD in the best docked pose (Fig. 5; Fig. 6; Table 2).

Phytochemical P4, Mogoltadone, has docking binding energy with prepared crystal structure of RVFV-CBD of -9.2 kcal/mol. In the best docked pose or CBD-P4 complex, P4 forms hydrophobic interactions with Y1728, P1755, V1727, M1782, F1713 and R1716 residues. Further, P4 forms aromatic interactions with F1713 and Y1728 residues of RVFV-CBD in the best docked pose (Fig. 5; Fig. 6; Table 2).

Phytochemical P5, Assafoetidnol A, has docking binding energy with prepared crystal structure of RVFV-CBD of -9.2 kcal/mol. In the best docked pose or CBD-P5 complex, P5 forms a hydrogen bond with Y1728 residue of RVFV-CBD. Further P5 forms hydrophobic interactions with Y1728, P1755, V1727, M1782, F1713 and R1716 residues. Moreover, P5 forms aromatic interactions with F1713 and Y1728 residues of RVFV-CBD in the best docked pose (Fig. 5; Fig. 6; Table 2).

Phytochemical P6, Kanzonol B is a chalcone that has docking binding energy with prepared crystal structure of RVFV-CBD of -8.9 kcal/mol. In the best docked pose or CBD-P6 complex, P6 forms a hydrogen bond interaction with the N1749 residue of RVFV-CBD. Further, P6 forms hydrophobic interaction with Y1728, M1782, F1713, R1716, P1755 residues. Moreover, P6 forms aromatic interactions with F1713 and Y1728 residues of RVFV-CBD in the best docked pose (Fig. 5; Fig. 6; Table 2).

Phytochemical P7, Gummosin, has docking binding energy with prepared crystal structure of RVFV-CBD of -8.6 kcal/mol. In the best docked pose or CBD-P7 complex, P7 forms a hydrogen bond with Y1728 residue of RVFV-CBD. Further, P7 forms hydrophobic interactions with F1713, P1755, M1782, Y1728, R1716 and Q1717 residues. Moreover, P7 also forms two aromatic interactions with F1713 and Y1728 residues of RVFV-CBD in the best docked pose (Fig. 5; Fig. 6; Table 2).

Phytochemical P8, Lupinisolone A is an isoflavonoid that has docking binding energy with prepared crystal structure of RVFV-CBD of -8.3 kcal/mol. Previously, isoflavonoids have been shown to have antiviral activity against herpes simplex virus [87] and SARS-CoV-2 [88]. In the best docked pose or CBD-P8 complex, P8 forms hydrophobic interactions with G1752, V1727, Y1728, M1782 and F1713 residues. Further, P8 forms one aromatic interaction with the active site residue Y1728 of RVFV-CBD in the best docked pose (Fig. 5; Fig. 6; Table 2).

Phytochemical P9, 7-Oxostigmasterol is a steroid that has docking binding energy with prepared crystal structure of RVFV-CBD of -8.1 kcal/mol. In the best docked pose or CBD-P9 complex, P9 forms hydrophobic interactions with Y1728, P1755, M1782, V1727, G1752 and F1713 residues of RVFV-CBD (Fig. 5; Fig. 6; Table 2).

MD based stability analysis of the RVFV-CBD in complex with top phytochemical hits

We assessed the stability of the protein-ligand complex for each of the top 9 phytochemicals by performing 150 ns of MD simulations for each complex. For each of the 9 phytochemicals, we initially ran the MD simulations in duplicates (2 replicas). The ligand in the protein-ligand complex was considered to be stable if both the replicas were stable during the MD simulation. Further, to confirm our observation for the ligand that was unstable in at least one of the replicas in the first round of MD simulations, the protein-ligand complex was subjected to another round of 150 ns MD simulations in duplicate (2 replicas). We considered a ligand in the protein-ligand complex to be stable, if both the replicas were stable, otherwise, the complex was considered to be unstable. Using this approach, we found that 4 phytochemicals namely, P1, P2, P7 and P8, among the top 9 hits are unstable in the protein-ligand complex during the MD simulations (**Figure S1**). The remaining 5 phytochemicals namely, P3, P4, P5, P6 and P9, are observed to be stable in the protein-ligand complex during the MD simulations (Fig. 7; Table 3).

Table 3
Five potential phytochemical inhibitors of RVFV-CBD whose protein-ligand complexes are stable during 150 ns MD simulations of the complexes. For each phytochemical, the table provides the chemical name along with the binding energy in kcal/mol of the ligand obtained from molecular docking and MM-PBSA based computation, in the best docked pose with the prepared crystal structure.

Phytochemical symbol	Chemical name	Docking binding energy (kcal/mol)	MM-PBSA binding energy (kcal/mol)
P3	Farnesiferol A	-9.3	-17.38 ± 3.91
P4	Mogoltadone	-9.2	-21.30 ± 3.02
P5	Assafoetidnol A	-9.2	-19.99 ± 5.07
P6	Kanzonol B	-8.9	-15.26 ± 2.11
P9	7-Oxostigmasterol	-8.1	-22.45 ± 3.53

Figure 7 shows the analysis of the trajectories from 150 ns of MD simulations of the protein-ligand complexes for 5 phytochemicals namely, P3, P4, P5, P6 and P9, which were ascertained to be stable during MD simulations. For the 5 phytochemicals, we observed that the RMSD of C_α atoms in the amino acids of the protein in the protein-ligand complex is stable throughout the simulation (Fig. 7a). The average RMSD values of the C_α atoms in RVFV-CBD in the complexes, CBD-P3 = 1.93 ± 0.42 Å, CBD-P4 = 2.91 ± 0.75 Å, CBD-P5 = 2.74 ± 0.51 Å, CBD-P6 = 2.84 ± 0.53 Å and CBD-P9 = 2.30 ± 0.42 Å. Further, the R_g for the complete protein structure was found to be stable throughout the simulation for the 5 phytochemicals (Fig. 7b), which suggests that the compactness of the protein is not affected by ligand binding. The average R_g values for the complexes, CBD-P3 = 14.55 ± 0.11 Å, CBD-P4 = 14.61 ± 0.12 Å,

CBD-P5 = 14.64 ± 0.12 Å, CBD-P6 = 14.54 ± 0.13 Å and CBD-P9 = 14.39 ± 0.11 Å. Moreover, the RMSF values of the amino acid residues of the RVFV-CBD in the protein-ligand complexes for the 5 phytochemicals are stable throughout the simulation and closely follow the RMSF values in the free protein simulation of the RVFV-CBD (Fig. 7c; Fig. 3c). Lastly, the RMSD of the heavy atoms of the phytochemical in the protein-ligand complexes for the 5 phytochemicals show that the 5 phytochemicals are stable during the MD simulations (Fig. 7d).

MM-PBSA based approach is a widely-used method to compute the binding energy of a ligand in protein-ligand complexes. Notably, the MM-PBSA based binding energies are considered to be more accurate than docking based binding energies [89]. Therefore, we computed the binding energy of the 5 potential phytochemical inhibitors in their corresponding protein-ligand complexes using the MM-PBSA approach (Methods; Table 3). The computed MM-PBSA binding energy for P3 in CBD-P3 complex is -17.38 ± 3.91 kcal/mol, P4 in CBD-P4 complex is -21.30 ± 3.02 kcal/mol, P5 in CBD-P5 is -19.99 ± 5.07 kcal/mol, P6 in CBD-P6 complex is -15.26 ± 2.11 kcal/mol, and P9 in CBD-P9 complex is -22.45 ± 3.53 kcal/mol (Table 3).

Conclusion

Re-emergence of certain diseases once considered eradicated in the 21st century has sparked world-wide concern and caught the attention of various stakeholders in public health. Rift Valley fever caused by RVFV is one such disease identified by the WHO as a disease of concern. Initially endemic to African region, RVFV has spread to countries like Saudi Arabia, Yemen, and recently, to Mauritania. If RVFV spreads to other regions, it may lead to massive economic loss and cause panic among the general populace. As recommended by the WHO, research and development towards therapeutics and vaccines against RVFV is critical to combat another possible looming pandemic.

Natural products or natural product-derived molecules have made monumental contributions to drug discovery. Medicinal plants used in traditional medicine remain an untapped resource for identifying potential drugs against emerging viral diseases. In case of RVFV, the cap-binding domain of L protein plays a vital role in viral transcription and is an ideal target for development of potential drugs. In this study, we attempted to identify phytochemical inhibitors against the CBD of RVFV L protein by employing multiple computational approaches. From a library of 14011 phytochemicals, we identified the subset of potential drug-like phytochemicals, and thereafter, docked the drug-like phytochemicals against the protein structures of RVFV-CBD. From the docking results, we used several filtering criteria such as non-covalent interaction filter and toxicity filter to identify 9 phytochemicals hits (P1-P9) for RVFV-CBD. Furthermore, using MD simulations, we assessed the stability of the 9 phytochemical hits in their corresponding protein-ligand complexes, and found that 5 phytochemicals are stable throughout the MD simulations. The 5 phytochemicals identified as promising and potential inhibitors of RVFV-CBD, can be sourced from Indian medicinal plants which have been used in traditional Indian systems of medicine. In conclusion, this work is a purely computational study with the aim of identifying potential phytochemical inhibitors from Indian herbs against RVFV infection. The promising phytochemical inhibitors predicted by

this computational study require additional validation against RVFV using wet lab experiments before the hits can be taken further in the drug discovery pipeline.

Declarations

Acknowledgements

The authors acknowledge the use of the high performance computing machine Nandadevi at The Institute of Mathematical Sciences, Chennai for molecular dynamics simulations. Areejit Samal would like to acknowledge funding from the Department of Atomic Energy (DAE), Government of India, and the Max Planck Society Germany (through the award of a Max Planck Partner Group). The funders have no role in study design, data collection, data analysis, manuscript preparation or decision to publish.

Author Contributions

Ishwarya Muralitharan: Conceptualization, Methodology, Formal Analysis, Visualization, Software, Writing; **Ajaya Kumar Sahoo:** Conceptualization, Methodology, Formal Analysis, Visualization, Software, Writing; **Priya Dharshini Augusthian:** Visualization, Writing; **Areejit Samal:** Conceptualization, Methodology, Formal Analysis, Supervision, Writing.

Funding

The authors did not receive any specific funding to carry out this research.

Conflict of interest

The authors declare that they have no conflicts of interest.

Data availability

Relevant data associated with this study is contained within the article or in supplementary Information.

Code availability

Not applicable.

Ethics approval

This is a purely computational study and ethics approvals are not applicable.

Consent to participate

Not applicable.

Consent for publication

All co-authors have read and approved the manuscript.

References

1. Ikegami T, Makino S (2011) The Pathogenesis of Rift Valley Fever. Viruses 3:493–519. https://doi.org/10.3390/v3050493
2. Hartman A (2017) Rift Valley Fever. Clin Lab Med 37:285–301. https://doi.org/10.1016/j.cll.2017.01.004
3. Ikegami T (2012) Molecular biology and genetic diversity of Rift Valley fever virus. Antivir Res 95:293–310. https://doi.org/10.1016/j.antiviral.2012.06.001
4. Baba M, Masiga DK, Sang R, Villinger J (2019) Has Rift Valley fever virus evolved with increasing severity in human populations in East Africa? Emerg Microbes Infect 5:1–10. https://doi.org/10.1038/emi.2016.57
5. Wright D, Kortekaas J, Bowden TA, Warimwe GM (2019) Rift Valley fever: biology and epidemiology. J Gen Virol 100:1187–1199. https://doi.org/10.1099/jgv.0.001296
6. Ganaie SS, Schwarz MM, McMillen CM, et al (2021) Lrp1 is a host entry factor for Rift Valley fever virus. Cell 184:5163–5178.e24. https://doi.org/10.1016/j.cell.2021.09.001
7. Al-Hazmi M, Ayoola EA, Abdurahman M, et al (2003) Epidemic Rift Valley Fever in Saudi Arabia: A Clinical Study of Severe Illness in Humans. Clin Infect Dis 36:245–252. https://doi.org/10.1086/345671
8. Madani TA, Al-Mazrou YY, Al-Jeffri MH, et al (2003) Rift Valley Fever Epidemic in Saudi Arabia: Epidemiological, Clinical, and Laboratory Characteristics. Clin Infect Dis 37:1084–1092. https://doi.org/10.1086/378747
9. Abdo-Salem S, Gerbier G, Bonnet P, et al (2006) Descriptive and Spatial Epidemiology of Rift Valley Fever Outbreak in Yemen 2000–2001. Ann N Y Acad Sci 1081:240–242. https://doi.org/10.1196/annals.1373.028
10. Mehand MS, Al-Shorbaji F, Millett P, Murgue B (2018) The WHO R&D Blueprint: 2018 review of emerging infectious diseases requiring urgent research and development efforts. Antivir Res 159:63–67. https://doi.org/10.1016/j.antiviral.2018.09.009
11. WHO (2018) 2018 Annual review of diseases prioritized under the Research and Development Blueprint
12. Cossaboom CM, Nyakarahuka L, Mulei S, et al (2022) Rift Valley Fever Outbreak during COVID-19 Surge, Uganda, 2021. Emerg Infect Dis 28:2290–2293. https://doi.org/10.3201/eid2811.220364
13. WHO (2022) Rift Valley fever - Mauritania. https://www.who.int/emergencies/disease-outbreak-news/item/2022-DON417. Accessed 8 Nov 2022
14. Nielsen SS, Alvarez J, Bicout DJ, et al (2020) Rift Valley Fever – epidemiological update and risk of introduction into Europe. EFSA Journal 18:6041. https://doi.org/10.2903/j.efsa.2020.6041

15. Bird BH, Ksiazek TG, Nichol ST, MacLachlan NJ (2009) Rift Valley fever virus. Journal of the American Veterinary Medical Association 234:883–893. https://doi.org/10.2460/javma.234.7.883
16. Rabinowitz P, Gordon Z, Chudnov D, et al (2006) Animals as Sentinels of Bioterrorism Agents. Emerg Infect Dis 12:647–652. https://doi.org/10.3201/eid1204.051120
17. Dar O, Hogarth S, McIntyre S (2013) Tempering the risk: Rift Valley fever and bioterrorism. Trop Med Int Health 18:1036–1041. https://doi.org/10.1111/tmi.12108
18. Dar O, McIntyre S, Hogarth S, Heymann D (2013) Rift Valley fever and a new paradigm of research and development for zoonotic disease control. Emerg Infect Dis 19:189–193. https://doi.org/10.3201/eid1902.120941
19. Geerling E, Murphy V, Mai MC, et al (2022) Metal coordinating inhibitors of Rift Valley fever virus replication. PLoS ONE 17:e0274266. https://doi.org/10.1371/journal.pone.0274266
20. Faburay B, Wilson W, McVey DS, et al (2013) Rift Valley Fever Virus Structural and Nonstructural Proteins: Recombinant Protein Expression and Immunoreactivity Against Antisera from Sheep. Vector Borne Zoonotic Dis 13:619–629. https://doi.org/10.1089/vbz.2012.1285
21. Giorgi C, Accardi L, Nicoletti L, et al (1991) Sequences and coding strategies of the S RNAs of Toscana and Rift Valley fever viruses compared to those of Punta Toro, Sicilian Sandfly fever, and Uukuniemi viruses. Virology 180:738–753. https://doi.org/10.1016/0042-6822(91)90087-r
22. Liu L, Celma CC, Roy P (2008) Rift Valley fever virus structural proteins: expression, characterization and assembly of recombinant proteins. Virol J 5:82. https://doi.org/10.1186/1743-422X-5-82
23. Gerrard SR, Nichol ST (2007) Synthesis, proteolytic processing and complex formation of N-terminally nested precursor proteins of the Rift Valley fever virus glycoproteins. Virology 357:124–133. https://doi.org/10.1016/j.virol.2006.08.002
24. Boshra H, Lorenzo G, Busquets N, Brun A (2011) Rift Valley Fever: Recent Insights into Pathogenesis and Prevention. J Virol 85:6098–6105. https://doi.org/10.1128/JVI.02641-10
25. Lopez N, Muller R, Prehaud C, Bouloy M (1995) The L protein of Rift Valley fever virus can rescue viral ribonucleoproteins and transcribe synthetic genome-like RNA molecules. J Virol 69:3972–3979. https://doi.org/10.1128/jvi.69.7.3972-3979.1995
26. Gogrefe N, Reindl S, Günther S, Rosenthal M (2019) Structure of a functional cap-binding domain in Rift Valley fever virus L protein. PLoS Pathog 15:e1007829. https://doi.org/10.1371/journal.ppat.1007829
27. Alamri MA, Mirza MU, Adeel MM, et al (2022) Structural Elucidation of Rift Valley Fever Virus L Protein towards the Discovery of Its Potential Inhibitors. Pharmaceuticals 15:659. https://doi.org/10.3390/ph15060659
28. Olschewski S, Cusack S, Rosenthal M (2020) The Cap-Snatching Mechanism of Bunyaviruses. Trends Microbiol 28:293–303. https://doi.org/10.1016/j.tim.2019.12.006
29. Reguera J, Weber F, Cusack S (2010) Bunyaviridae RNA Polymerases (L-Protein) Have an N-Terminal, Influenza-Like Endonuclease Domain, Essential for Viral Cap-Dependent Transcription. PLoS Pathog 6:e1001101. https://doi.org/10.1371/journal.ppat.1001101

30. Benedict A, Bansal N, Senina S, et al (2015) Repurposing FDA-approved drugs as therapeutics to treat Rift Valley fever virus infection. Front Microbiol 6:676. https://doi.org/10.3389/fmicb.2015.00676
31. Keck F, Amaya M, Kehn-Hall K, et al (2015) Characterizing the effect of Bortezomib on Rift Valley Fever Virus multiplication. Antivir Res 120:48–56. https://doi.org/10.1016/j.antiviral.2015.05.004
32. Broce S, Hensley L, Sato T, et al (2016) Biochemical and biophysical characterization of cell-free synthesized Rift Valley fever virus nucleoprotein capsids enables in vitro screening to identify novel antivirals. Biol Direct 11:25. https://doi.org/10.1186/s13062-016-0126-5
33. Islam MdK, Baudin M, Eriksson J, et al (2016) High-Throughput Screening Using a Whole-Cell Virus Replication Reporter Gene Assay to Identify Inhibitory Compounds against Rift Valley Fever Virus Infection. SLAS Discov 21:354–362. https://doi.org/10.1177/1087057115625184
34. Brahms A, Mudhasani R, Pinkham C, et al (2017) Sorafenib Impedes Rift Valley Fever Virus Egress by Inhibiting Valosin-Containing Protein Function in the Cellular Secretory Pathway. J Virol 91:e00968-17. https://doi.org/10.1128/JVI.00968-17
35. Fatima I, Ahmad S, Alamri MA, et al (2022) Discovery of Rift Valley fever virus natural pan-inhibitors by targeting its multiple key proteins through computational approaches. Scientific Reports 12:9260. https://doi.org/10.1038/s41598-022-13267-1
36. Lin L-T, Hsu W-C, Lin C-C (2014) Antiviral Natural Products and Herbal Medicines. Journal of Traditional and Complementary Medicine 4:24–35. https://doi.org/10.4103/2225-4110.124335
37. Ben-Shabat S, Yarmolinsky L, Porat D, Dahan A (2020) Antiviral effect of phytochemicals from medicinal plants: Applications and drug delivery strategies. Drug Deliv and Transl Res 10:354–367. https://doi.org/10.1007/s13346-019-00691-6
38. Mohanraj K, Karthikeyan BS, Vivek-Ananth RP, et al (2018) IMPPAT: A curated database of Indian Medicinal Plants, Phytochemistry And Therapeutics. Scientific Reports 8:4329. https://doi.org/10.1038/s41598-018-22631-z
39. Basu A, Sarkar A, Maulik U (2020) Molecular docking study of potential phytochemicals and their effects on the complex of SARS-CoV2 spike protein and human ACE2. Scientific Reports 10:17699. https://doi.org/10.1038/s41598-020-74715-4
40. Borkotoky S, Banerjee M (2021) A computational prediction of SARS-CoV-2 structural protein inhibitors from Azadirachta indica (Neem). Journal of Biomolecular Structure and Dynamics 39:4111–4121. https://doi.org/10.1080/07391102.2020.1774419
41. Vivek-Ananth RP, Krishnaswamy S, Samal A (2022) Potential phytochemical inhibitors of SARS-CoV-2 helicase Nsp13: a molecular docking and dynamic simulation study. Molecular Diversity 26:429–442. https://doi.org/10.1007/s11030-021-10251-1
42. Vivek-Ananth RP, Sahoo AK, Srivastava A, Samal A (2022) Virtual screening of phytochemicals from Indian medicinal plants against the endonuclease domain of SFTS virus L polymerase. RSC Adv 12:6234–6247. https://doi.org/10.1039/D1RA06702H

43. Chatterjee A, Pakrashi SC (1991) The treatise on Indian medicinal plants, Vol 1. Publications & Information Directorate, Council of Scientific & Industrial Research (India), New Delhi
44. Chatterjee A, Pakrashi SC (1992) The treatise on Indian medicinal plants, Vol 2. Publications & Information Directorate, Council of Scientific & Industrial Research (India), New Delhi
45. Chatterjee A, Pakrashi SC (1994) The treatise on Indian medicinal plants, Vol 3. Publications & Information Directorate, Council of Scientific & Industrial Research (India), New Delhi
46. Chatterjee A, Pakrashi SC (1995) The treatise on Indian medicinal plants, Vol 4. Publications & Information Directorate, Council of Scientific & Industrial Research (India), New Delhi
47. Chatterjee A, Pakrashi SC (1997) The treatise on Indian medicinal plants, Vol 5. Publications & Information Directorate, Council of Scientific & Industrial Research (India), New Delhi
48. The Wealth of India (2000) The wealth of India: A dictionary of Indian raw materials & industrial products, Vol 1. National Institute of Science Communication, Council of Scientific & Industrial Research, New Delhi
49. The Wealth of India (2000) The wealth of India: A dictionary of Indian raw materials & industrial products, Vol 2. National Institute of Science Communication, Council of Scientific & Industrial Research, New Delhi
50. The Wealth of India (2000) The wealth of India: A dictionary of Indian raw materials & industrial products, Vol 3. National Institute of Science Communication, Council of Scientific & Industrial Research, New Delhi
51. The Wealth of India (2000) The wealth of India: A dictionary of Indian raw materials & industrial products, Vol 4. National Institute of Science Communication, Council of Scientific & Industrial Research, New Delhi
52. The Wealth of India (2000) The wealth of India: A dictionary of Indian raw materials & industrial products, Vol 5. National Institute of Science Communication, Council of Scientific & Industrial Research, New Delhi
53. Rastogi RP (1990) Compendium of Indian medicinal plants, Vol 1. Central Drug Research Institute, Lucknow
54. Rastogi RP (1991) Compendium of Indian medicinal plants, Vol 2. Central Drug Research Institute, Lucknow
55. Rastogi RP (1993) Compendium of Indian medicinal plants, Vol 3. Central Drug Research Institute, Lucknow
56. Rastogi RP (1995) Compendium of Indian medicinal plants, Vol 4. Central Drug Research Institute, Lucknow
57. Rastogi RP (1998) Compendium of Indian medicinal plants, Vol 5. Central Drug Research Institute, Lucknow
58. Lipinski CA, Lombardo F, Dominy BW, Feeney PJ (2001) Experimental and computational approaches to estimate solubility and permeability in drug discovery and development settings. Adv Drug Deliv

Rev 46:3–26. https://doi.org/10.1016/s0169-409x(00)00129-0

59. Kim S, Chen J, Cheng T, et al (2021) PubChem in 2021: new data content and improved web interfaces. Nucleic Acids Res 49:D1388–D1395. https://doi.org/10.1093/nar/gkaa971
60. O'Boyle NM, Banck M, James CA, et al (2011) Open Babel: An open chemical toolbox. J Cheminformatics 3:33. https://doi.org/10.1186/1758-2946-3-33
61. Pettersen EF, Goddard TD, Huang CC, et al (2004) UCSF Chimera–a visualization system for exploratory research and analysis. J Comput Chem 25:1605–1612. https://doi.org/10.1002/jcc.20084
62. Abraham MJ, Murtola T, Schulz R, et al (2015) GROMACS: High performance molecular simulations through multi-level parallelism from laptops to supercomputers. SoftwareX 1:19–25. https://doi.org/10.1016/j.softx.2015.06.001
63. Huang J, MacKerell ADJ (2013) CHARMM36 all-atom additive protein force field: validation based on comparison to NMR data. J Comput Chem 34:2135–2145. https://doi.org/10.1002/jcc.23354
64. Hess B, Bekker H, Berendsen HJ, Fraaije JG (1997) LINCS: a linear constraint solver for molecular simulations. J Comput Chem 18:1463–1472. https://doi.org/10.1002/(SICI)1096-987X(199709)18:12<1463::AID-JCC4>3.0.CO;2-H
65. Berendsen HJ, Postma J van, Van Gunsteren WF, et al (1984) Molecular dynamics with coupling to an external bath. J Chem Phys 81:3684–3690. https://doi.org/10.1063/1.448118
66. Parrinello M, Rahman A (1981) Polymorphic transitions in single crystals: A new molecular dynamics method. J Appl Phys 52:7182–7190. https://doi.org/10.1063/1.328693
67. Jarvis RA, Patrick EA (1973) Clustering Using a Similarity Measure Based on Shared Near Neighbors. IEEE Transactions on Computers C–22:1025–1034. https://doi.org/10.1109/T-C.1973.223640
68. Trott O, Olson AJ (2010) AutoDock Vina: improving the speed and accuracy of docking with a new scoring function, efficient optimization, and multithreading. J Comput Chem 31:455–461. https://doi.org/10.1002/jcc.21334
69. Morris GM, Huey R, Lindstrom W, et al (2009) AutoDock4 and AutoDockTools4: Automated docking with selective receptor flexibility. J Comput Chem 30:2785–2791. https://doi.org/10.1002/jcc.21256
70. DeLano WL (2002) The PyMOL molecular graphics system. http://www pymol org
71. Rodrigues JPGLM, Teixeira JMC, Trellet M, Bonvin AMJJ (2018) pdb-tools: a swiss army knife for molecular structures. F1000Res 7:1961. https://doi.org/10.12688/f1000research.17456.1
72. Vivek-Ananth RP, Rana A, Rajan N, et al (2020) In Silico Identification of Potential Natural Product Inhibitors of Human Proteases Key to SARS-CoV-2 Infection. Molecules 25:3822. https://doi.org/10.3390/molecules25173822
73. Sahoo AK, Augusthian PD, Muralitharan I, et al (2022) In silico identification of potential inhibitors of vital monkeypox virus proteins from FDA approved drugs. Molecular Diversity. https://doi.org/10.1007/s11030-022-10550-1

74. Zoete V, Cuendet MA, Grosdidier A, Michielin O (2011) SwissParam: A fast force field generation tool for small organic molecules. Journal of Computational Chemistry 32:2359–2368. https://doi.org/10.1002/jcc.21816
75. Baker NA, Sept D, Joseph S, et al (2001) Electrostatics of nanosystems: application to microtubules and the ribosome. Proc Natl Acad Sci USA 98:10037–10041. https://doi.org/10.1073/pnas.181342398
76. Kumari R, Kumar R, Lynn A (2014) g_mmpbsa–a GROMACS tool for high-throughput MM-PBSA calculations. J Chem Inf Model 54:1951–1962. https://doi.org/10.1021/ci500020m
77. Daina A, Michielin O, Zoete V (2017) SwissADME: a free web tool to evaluate pharmacokinetics, drug-likeness and medicinal chemistry friendliness of small molecules. Scientific Reports 7:42717. https://doi.org/10.1038/srep42717
78. Banerjee P, Eckert AO, Schrey AK, Preissner R (2018) ProTox-II: a webserver for the prediction of toxicity of chemicals. Nucleic Acids Research 46:W257–W263. https://doi.org/10.1093/nar/gky318
79. Djoumbou Feunang Y, Eisner R, Knox C, et al (2016) ClassyFire: automated chemical classification with a comprehensive, computable taxonomy. Journal of Cheminformatics 8:61. https://doi.org/10.1186/s13321-016-0174-y
80. Chopra RN, Nayar SL, Chopra LC (1996) Glossary of Indian medicinal plants. Publications & Information Directorate, National Institute of Science Communication, New Delhi, India
81. The Wealth of India (2000) The Wealth of India: A Dictionary of Indian Raw Materials & Industrial Products. First supplement series (Raw materials). National Institute of Science Communication, Council of Scientific & Industrial Research, New Delhi
82. Mahendra P, Bisht S (2012) Ferula asafoetida: Traditional uses and pharmacological activity. Pharmacogn Rev 6:141–146. https://doi.org/10.4103/0973-7847.99948
83. Akbar S (2020) Lupinus albus L. (Fabaceae/Leguminosae). In: Akbar S (ed) Handbook of 200 Medicinal Plants: A Comprehensive Review of Their Traditional Medical Uses and Scientific Justifications. Springer International Publishing, Cham, pp 1123–1128
84. Bavarva JH, Narasimhacharya AVRL (2010) Leucas cephalotes regulates carbohydrate and lipid metabolism and improves antioxidant status in IDDM and NIDDM rats. Journal of Ethnopharmacology 127:98–102. https://doi.org/10.1016/j.jep.2009.09.042
85. Das SN, Patro VJ, Dinda SC (2012) A review: Ethnobotanical survey of genus Leucas. Pharmacogn Rev 6:100–106. https://doi.org/10.4103/0973-7847.99943
86. Elkhalifa D, Al-Hashimi I, Al Moustafa A-E, Khalil A (2021) A comprehensive review on the antiviral activities of chalcones. J Drug Target 29:403–419. https://doi.org/10.1080/1061186X.2020.1853759
87. Arthan D, Svasti J, Kittakoop P, et al (2002) Antiviral isoflavonoid sulfate and steroidal glycosides from the fruits of Solanum torvum. Phytochemistry 59:459–463. https://doi.org/10.1016/s0031-9422(01)00417-4

88. Alesawy MS, Abdallah AE, Taghour MS, et al (2021) In Silico Studies of Some Isoflavonoids as Potential Candidates against COVID-19 Targeting Human ACE2 (hACE2) and Viral Main Protease (Mpro). Molecules 26:2806. https://doi.org/10.3390/molecules26092806
89. Genheden S, Ryde U (2015) The MM/PBSA and MM/GBSA methods to estimate ligand-binding affinities. Expert Opinion on Drug Discovery 10:449–461. https://doi.org/10.1517/17460441.2015.1032936

Figures

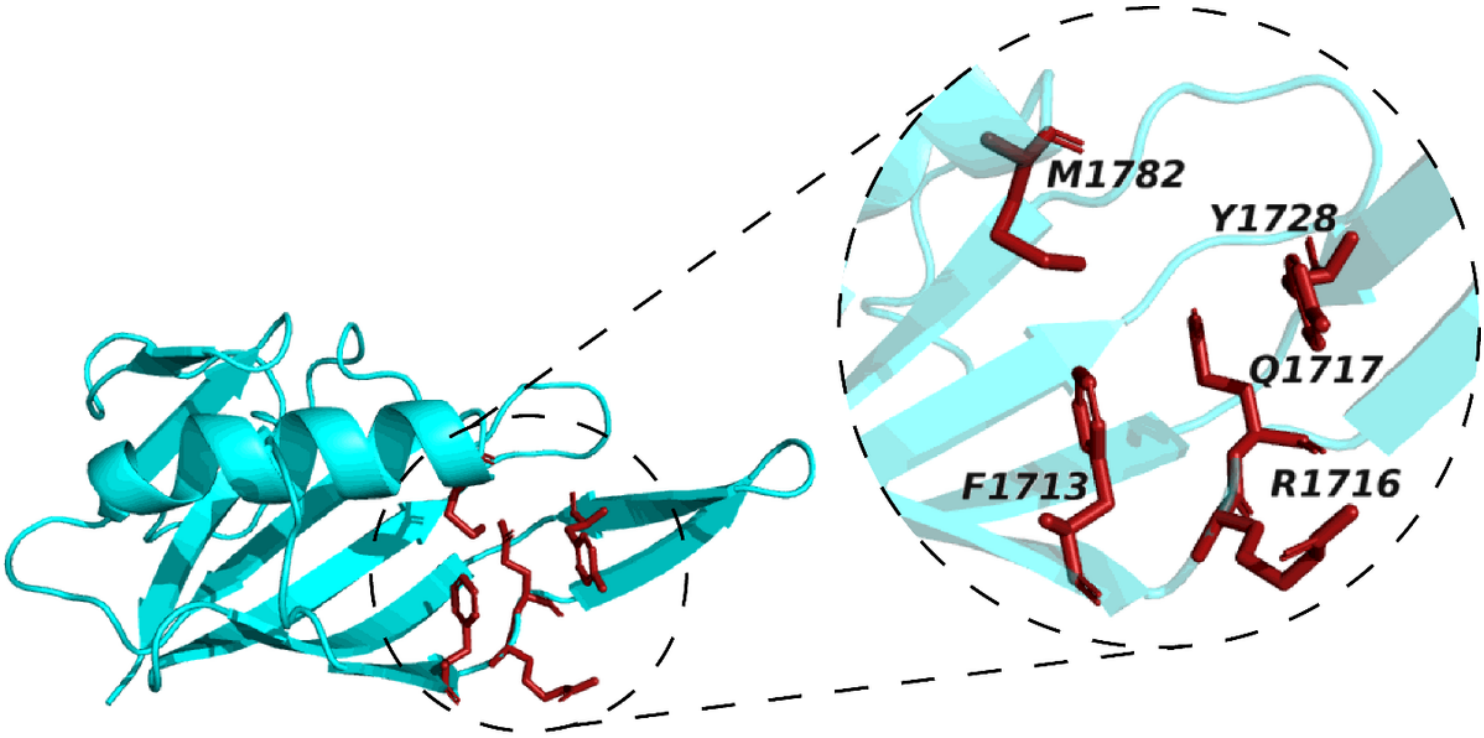

Figure 1

Cartoon representation of the prepared crystal structure of RVFV-CBD. The critical active site residues F1713, R1716, Q1717, Y1728 and M1782 are shown as red color sticks. The active site residues are also shown in an expanded view.

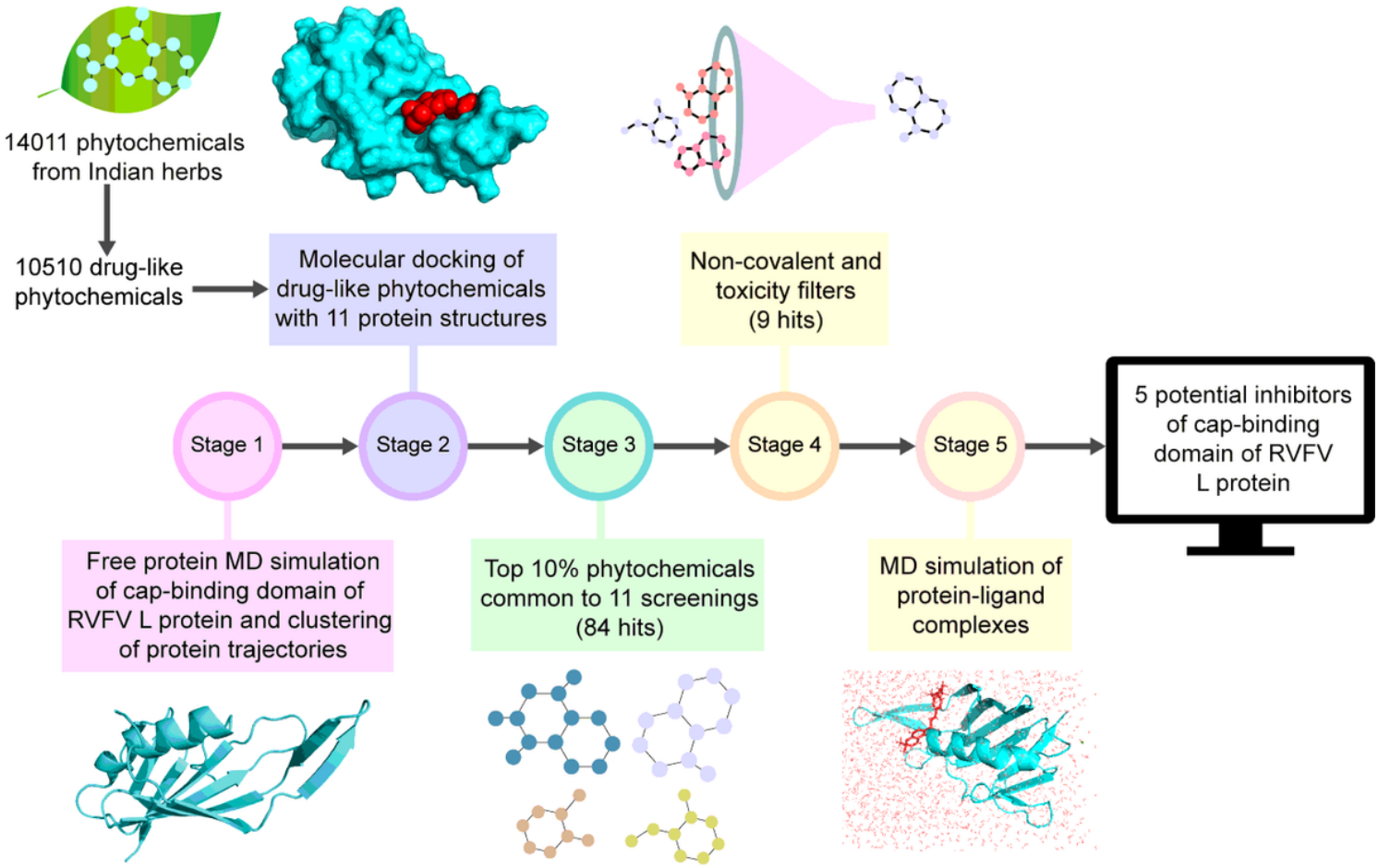

Figure 2

Schematic overview of the computational workflow comprising of five stages for the identification of potential phytochemical inhibitors of RVFV-CBD.

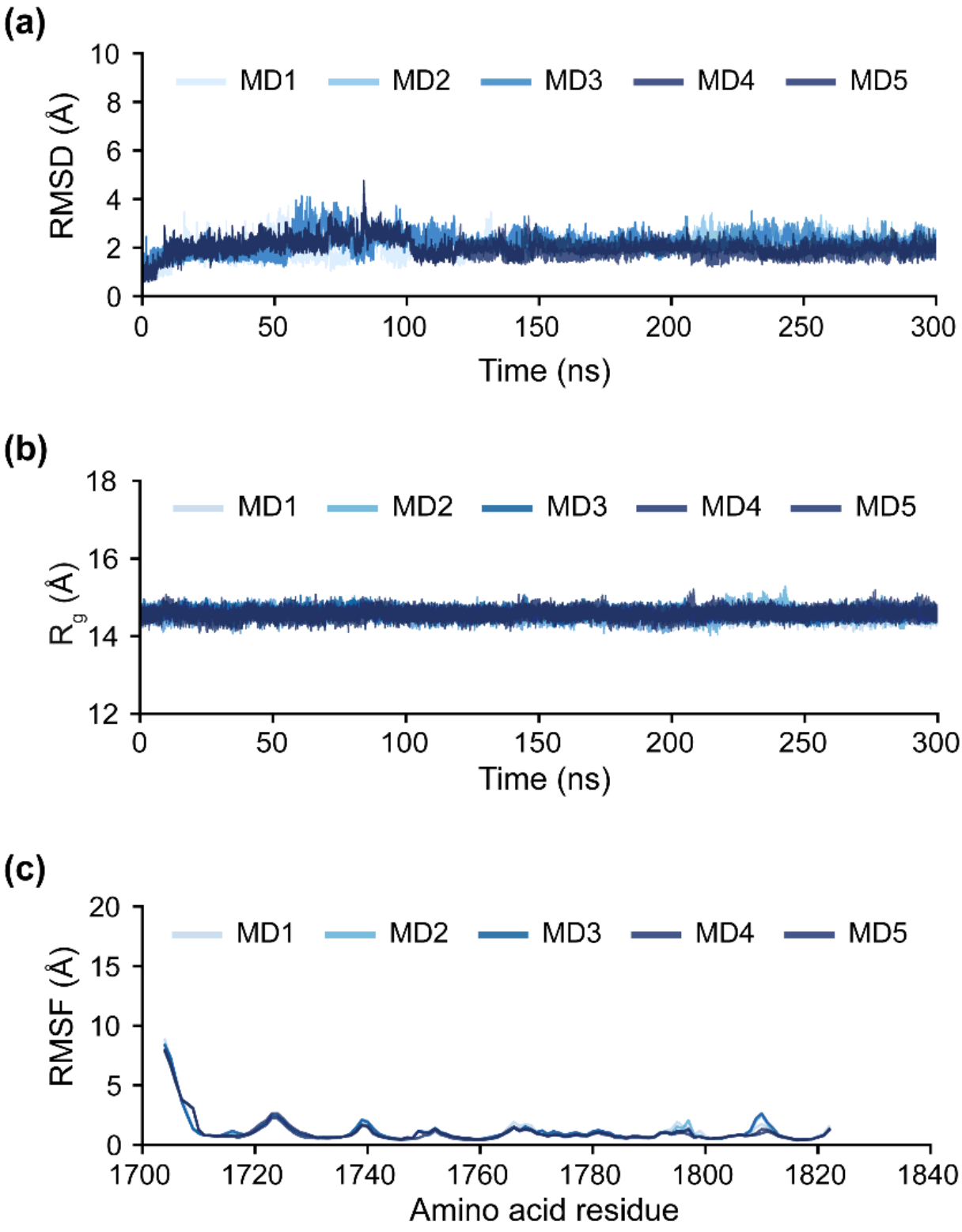

Figure 3

Analysis of the trajectory of the 300 ns MD simulation in quintuplicate for RVFV-CBD. (a) RMSD of the C_α atoms of amino acid residues in the protein. (b) Radius of gyration (R_g) of the complete protein structure. (c) RMSF of the C_α atoms of amino acid residues in the protein.

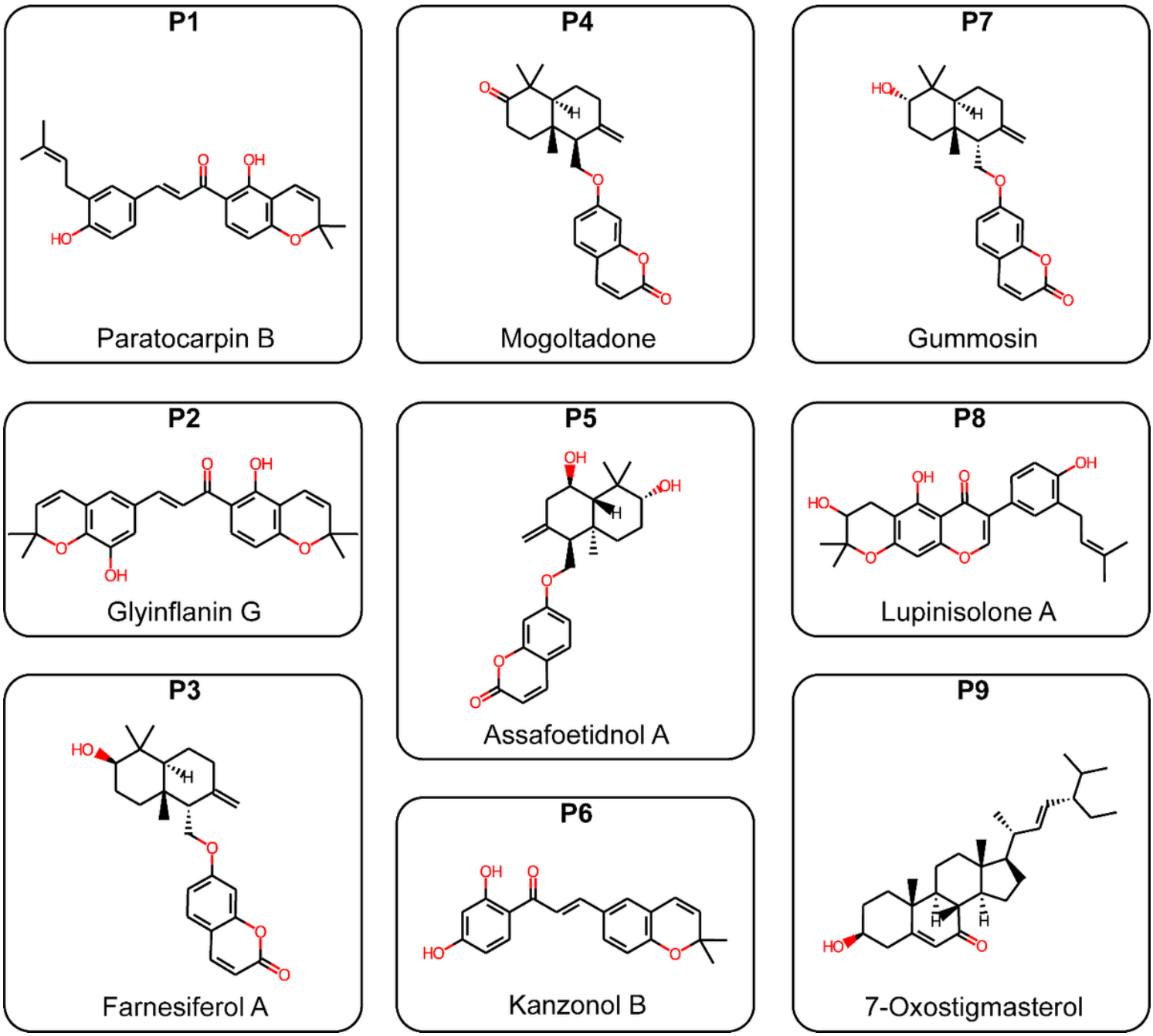

Figure 4

Top 9 phytochemical hits based on docking of RVFV-CBD. The figure displays the two-dimensional (2D) structures, symbols and names of the top 9 phytochemicals.

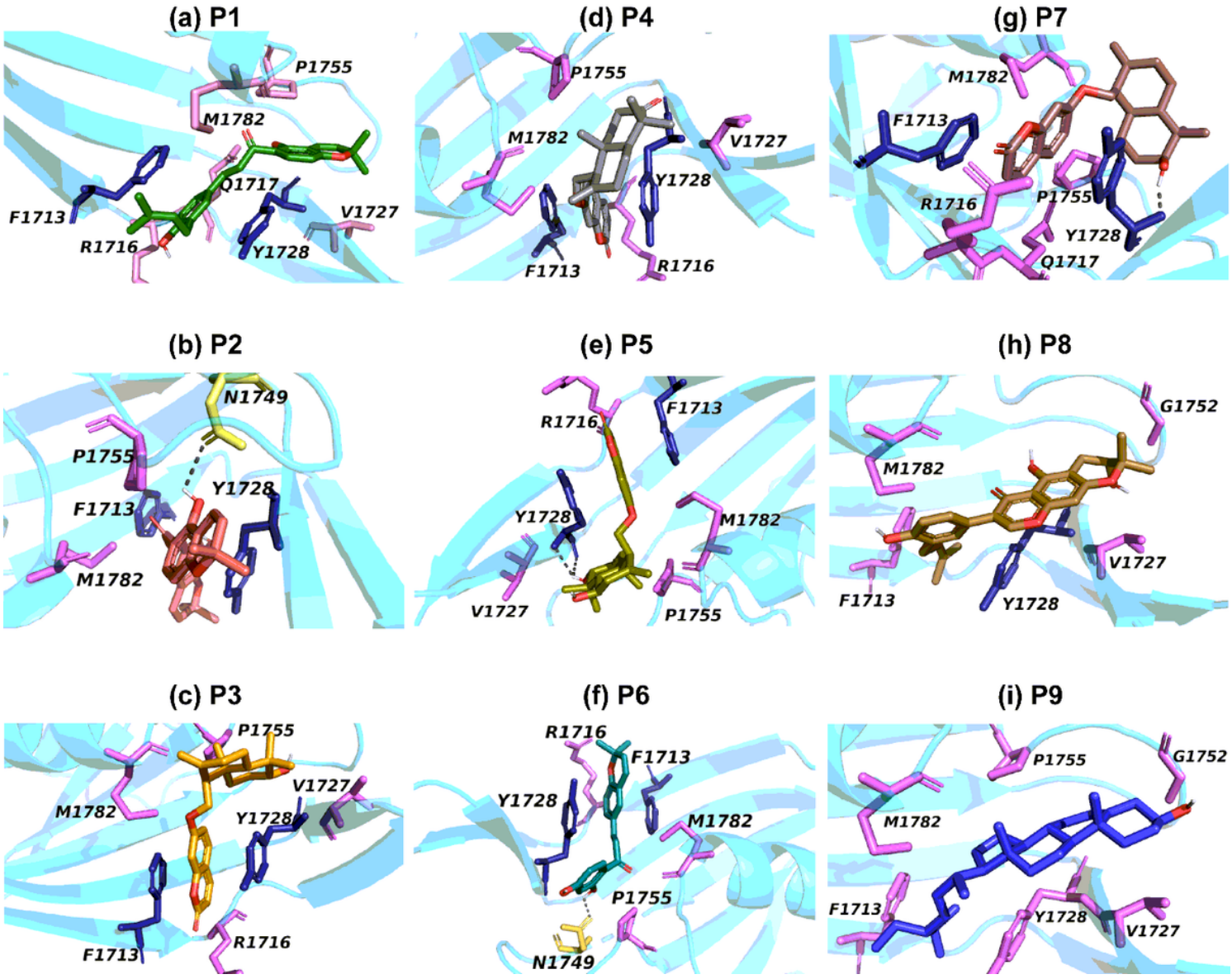

Figure 5

Three-dimensional (3D) cartoon representation of the interaction of the top 9 phytochemical hits (P1-P9) with the amino acid residues of RVFV-CBD. Note that, interactions are shown for the ligand in its best docked pose with the protein. For each case, the amino acid residues of the protein, which form aromatic interactions are shown in deep blue, which form hydrophobic interactions are shown in violet, and which form hydrogen bond interactions are shown in yellow. The hydrogen bond interactions are shown in grey dotted lines. The carbon atoms are shown in forest green for P1, salmon red for P2, yellow for P3, grey for P4, deep olive for P5, deep teal for P6, dirty violet for P7, yellow sand for P8, and blue for P9. The oxygen atoms for all the ligands are shown in red color.

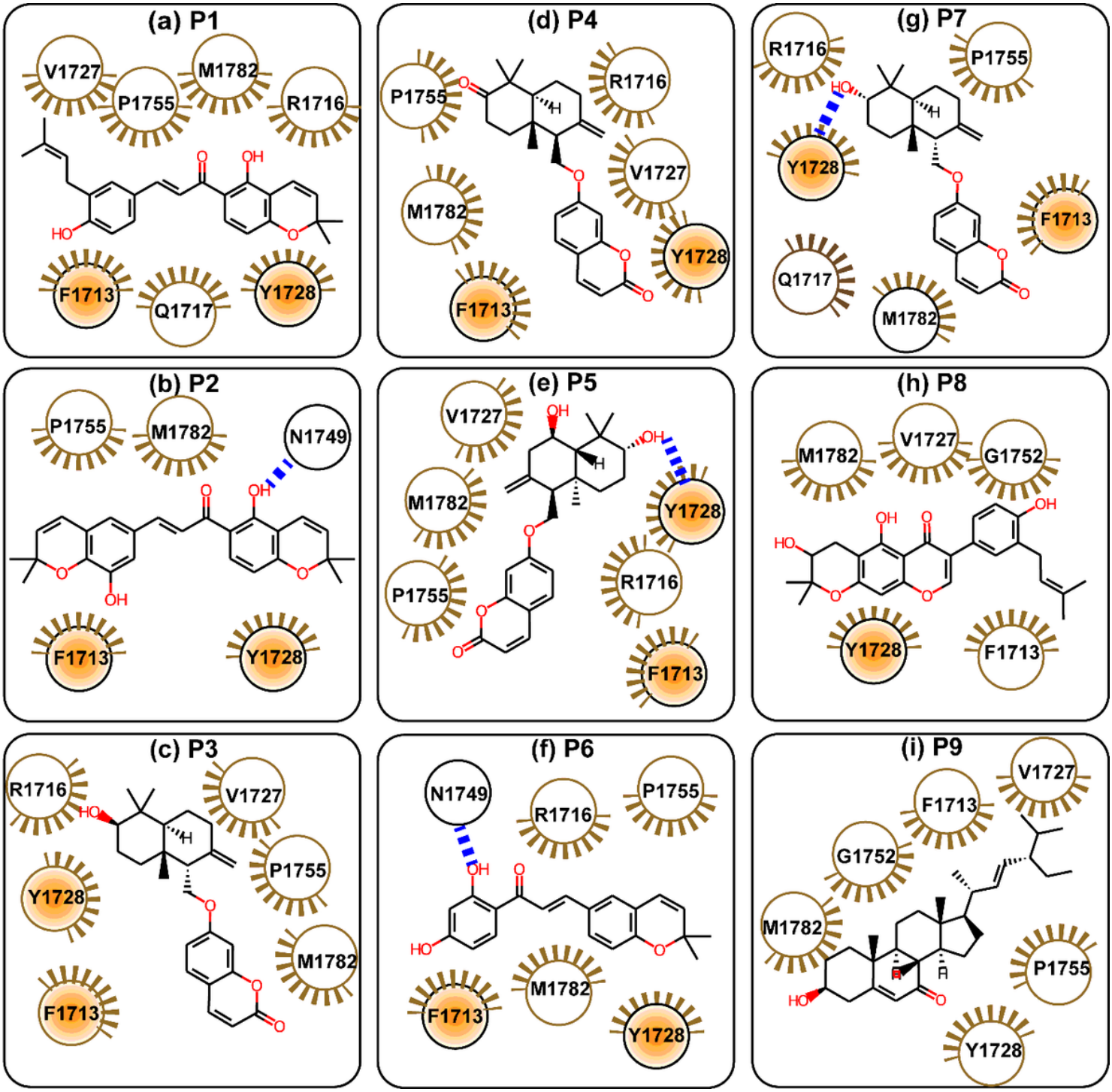

Figure 6

Two-dimensional (2D) cartoon representation of the interaction of the top 9 phytochemical hits (P1-P9) with the amino acid residues of RVFV-CBD. Note that, interactions are shown for the ligand in its best docked pose with the protein. For each case, the amino acid residues of the protein, which form aromatic interactions are shaded in orange, which form hydrophobic interactions are shown as spiked circular segments, and which form hydrogen bond interactions are shown as empty circles. Further the hydrogen bond interactions are shown by blue dashed lines.

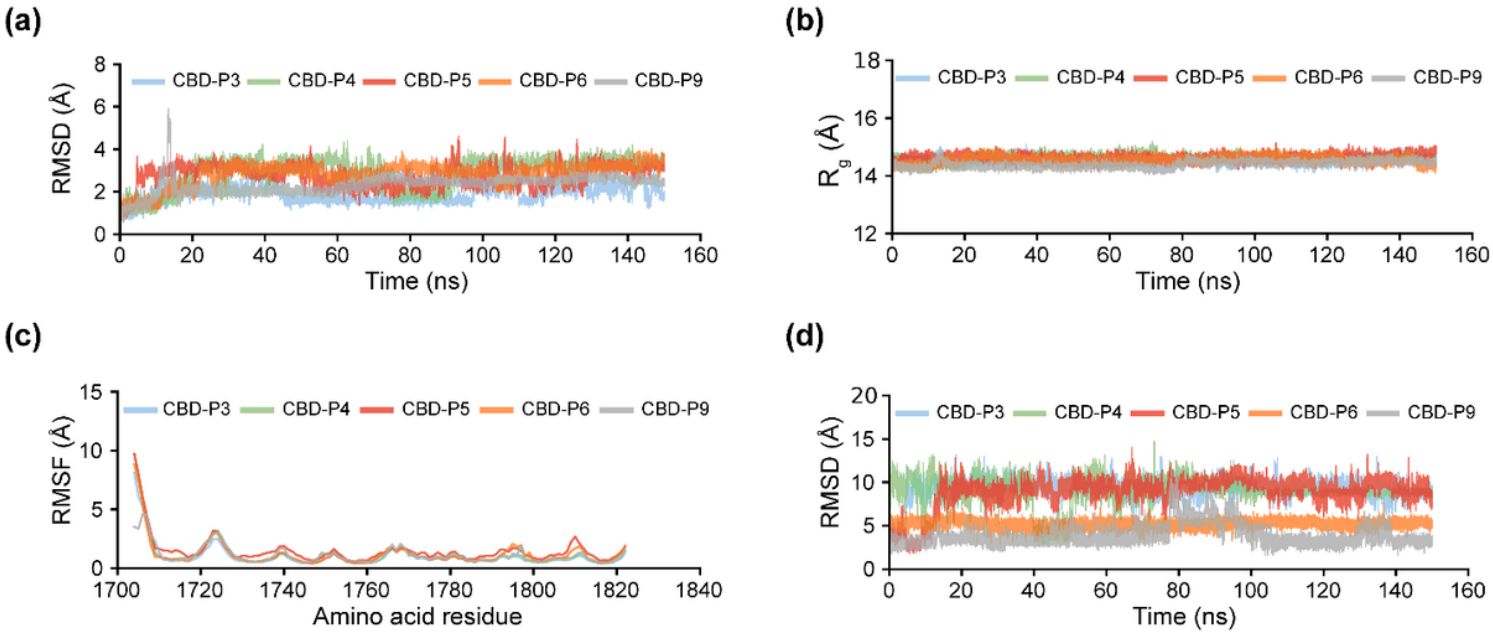

Figure 7

Analysis of the trajectories from 150 ns MD simulations of the five potential phytochemical inhibitors (P3, P4, P5, P6 and P9) in complex with RVFV-CBD. (a) RMSD of C_α atoms of the amino acid residues in the protein. (b) Radius of gyration (R_g) for the complete protein structure. (c) RMSF of C_α atoms of the amino acid residues in the protein. (d) RMSD of heavy atoms of the 5 potential phytochemical inhibitors (P3, P4, P5, P6 and P9).

Supplementary Files

This is a list of supplementary files associated with this preprint. Click to download.

- SupFiguresRVFV.docx
- SupTablesRVFV.xlsx
- SupplementaryInformation.docx